Supporting Information (SI) for:

Controlled Synthesis and Post-Modification of Polypentafluorostyrene in Continuous Flow

Alexander P. Grimm,[a] Amna B. Asghar,[b] Björn Schmidt,[a] Christian W. Schmitt,[a] Dominik Voll,[c] Tanja Junkers[b] and Patrick Théato[ac]*

[a] Institute for Biological Interfaces III (IBG-3), Karlsruhe Institute of Technology (KIT), Hermann-von-Helmholtz-Platz 1, 76344 Eggenstein-Leopoldshafen, Germany.

[b] Polymer Reaction Design Group, School of Chemistry, Monash University, 19 Rainforest Walk, Clayton, 3800 Victoria, Australia.

[c] Institute for Technical Chemistry and Polymer Chemistry (ITCP), Karlsruhe Institute of Technology (KIT), Engesserstr. 18, 76131 Karlsruhe, Germany.

Experimental

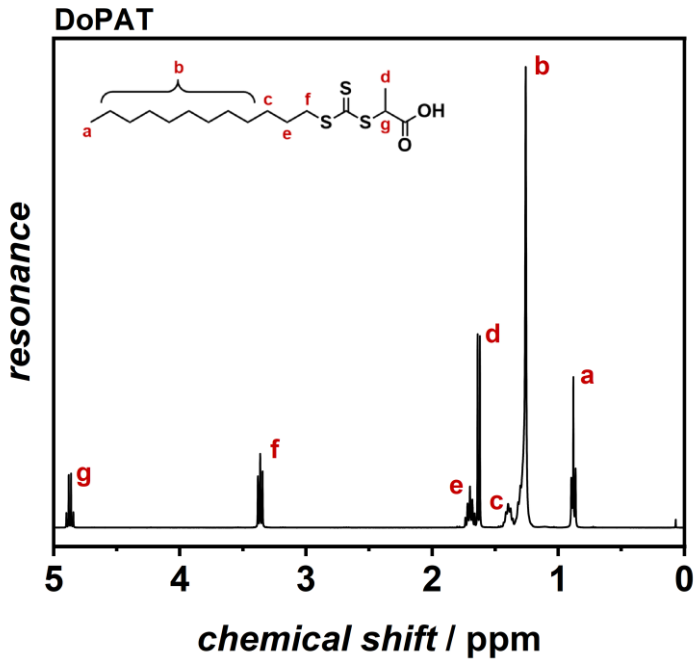

Figure S1. ^{1}H NMR spectrum of DoPAT in $CDCl_3$ in the range from 5 to 0 ppm. ^{1}H NMR (400 MHz, $CDCl_3$): δ (ppm) = 4.88 (quart., 1H, H**g**), 3.36 (t, 2H, H**f**), 1.70 (quint., 2H, H**e**), 1.64 (d, 3H, H**d**), 1.40 (m, 2H, H**c**), 1.26 (m, 16H, H**b**), 0.88 (t, 3H, H**a**).

Table S1. Flow rates of corresponding residence times used for the 4 timesweeps conducted in this work. The reactor was a tubular PTFE coil with a volume of 2 mL.

flow rate / mL min^{-1}	*residence time* / min
0.5	4
0.25	8
0.125	16
0.0625	32
0.0333	60

Table S2. Flow rates of polymer, thiol, and DBU solutions for the kinetic study of the PFTR of poly(PFSty) with DT, FBM, and TFBM, respectively. The reactor was a tubular PTFE coil with a volume of 2 mL.

polymer flow rate / mL min^{-1}	*thiol flow rate* / mL min^{-1}	*DBU flow rate* / mL min^{-1}	*total flow rate* / mL min^{-1}	*residence time* / min
0.50000	0.25000	0.25000	1.00000	1
0.25000	0.12500	0.12500	0.50000	2
0.16667	0.08333	0.08333	0.33333	3
0.08333	0.04167	0.04167	0.16667	6
0.05555	0.02778	0.02778	0.11111	9
0.04167	0.02083	0.02083	0.08333	12
0.03333	0.01667	0.01667	0.06667	15

Table S3. Flow rates of each reaction component of mixed flow-PFTRs. Investigated thiol mixtures were DT-FBM, DT-TFBM, and FBM-TFBM. The total flow rate was 0.2 mL min^{-1}, and the reactor volume was 1 mL, resulting in a residence time of 5 min for each sample.

thiol ratio / mol%	*polymer flow rate* / mL min^{-1}	*thiol 1 flow rate* / mL min^{-1}	*thiol 2 flow rate* / mL min^{-1}	*DBU flow rate* / mL min^{-1}
10/90	0.1	0.005	0.045	0.050
20/80	0.1	0.010	0.040	0.050
30/70	0.1	0.015	0.035	0.050
40/50	0.1	0.020	0.030	0.050
50/50	0.1	0.025	0.025	0.050
60/40	0.1	0.030	0.020	0.050
70/30	0.1	0.035	0.015	0.050
80/20	0.1	0.040	0.010	0.050
90/10	0.1	0.045	0.005	0.050

Results and discussion

Details on the automated reaction platform for TT experiments

The setup we used for our work is a fully automated flow chemistry system designed for high-throughput polymerisation screening and has previously described in more detail.[1] It incorporates a computer-controlled syringe pump to precisely deliver a pre-mixed solution of monomer, initiator, and solvent into a tubular flow reactor, where reaction conditions such as temperature and residence time are tightly regulated. An inline benchtop NMR spectrometer is positioned directly within the flow path to continuously monitor monomer conversion in real time, eliminating the need for manual sampling. Downstream, the system is equipped with an online SEC module that automatically samples the reaction output, quenches it if necessary, and performs molecular weight analysis (M_n, M_w, $Đ$) without interrupting the flow. Automated valve switching and cleaning routines ensure seamless sample routing and prevent contamination between experiments. All components are coordinated through an integrated software interface that handles experimental execution, hardware control, and automated data processing, enabling fully unattended operation and consistent data generation across multiple runs.

Table S4. Monomer conversion after 60 min residence time, apparent polymerisation rate coefficient, and respective linear fit qualities for the RAFT polymerisation of PFSty with varying RAFT agents.

RAFT-agent	*conversion after 60 min / %*	k_{app} / s^{-1}	*coefficient of determination* R^2
CPDT	41.7	$8.96 \cdot 10^{-3} \pm 5.72 \cdot 10^{-5}$	0.983
CDCTPA	27.0	$5.52 \cdot 10^{-3} \pm 4.53 \cdot 10^{-5}$	0.973
DoPAT	49.0	$1.05 \cdot 10^{-2} \pm 7.79 \cdot 10^{-5}$	0.978
CBCDMPC	36.7	$6.83 \cdot 10^{-3} \pm 8.77 \cdot 10^{-5}$	0.936

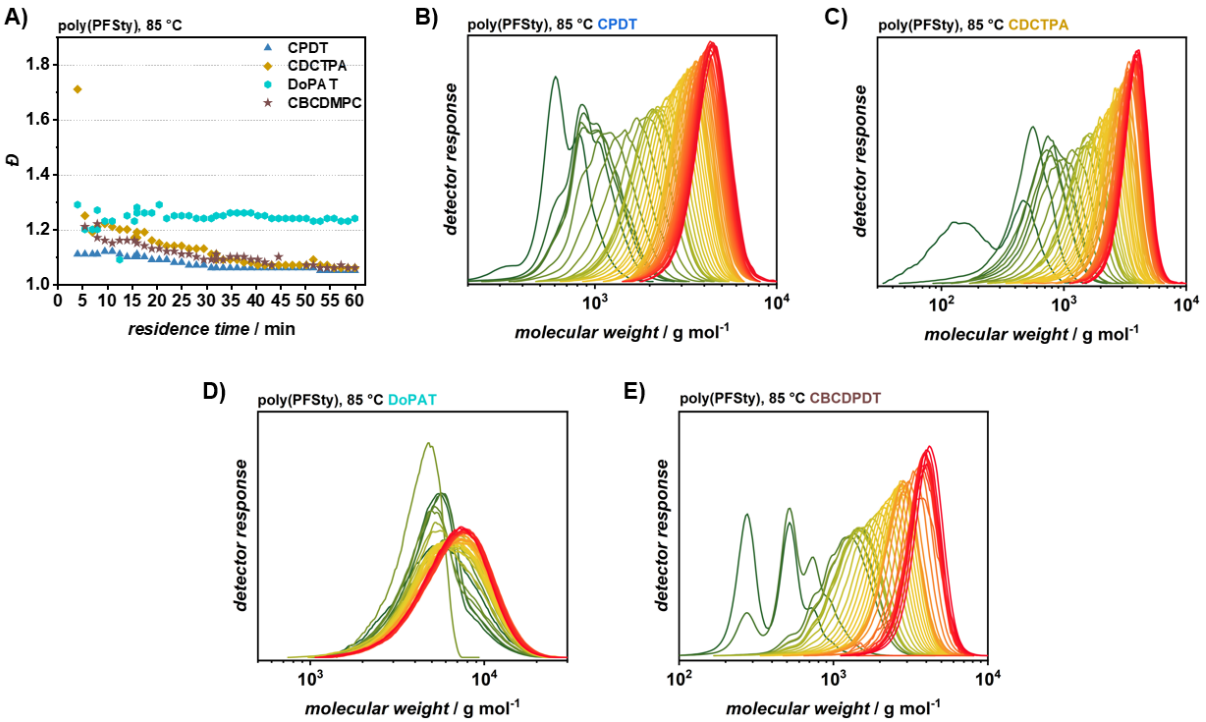

Figure S2. A) Evolution of *Đ* of poly(PFSty) with increasing residence time using different RAFT agents at 85 °C. DoPAT offered the least control over the polymerisation. B)-E) SEC traces of poly(PFSty) with increasing residence time (from green to red) recorded by online SEC using different RAFT agents at 85 °C. Calibration: PS.

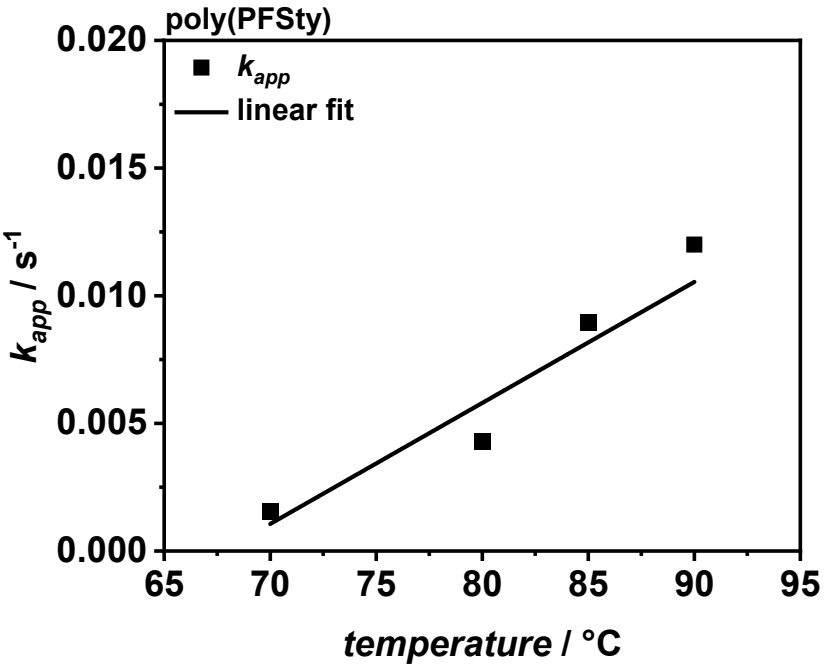

Figure S3. Apparent polymerisation rate coefficient k_{app} of the RAFT polymerisation of PFSty at different reaction temperatures with CPDT as RAFT agent.

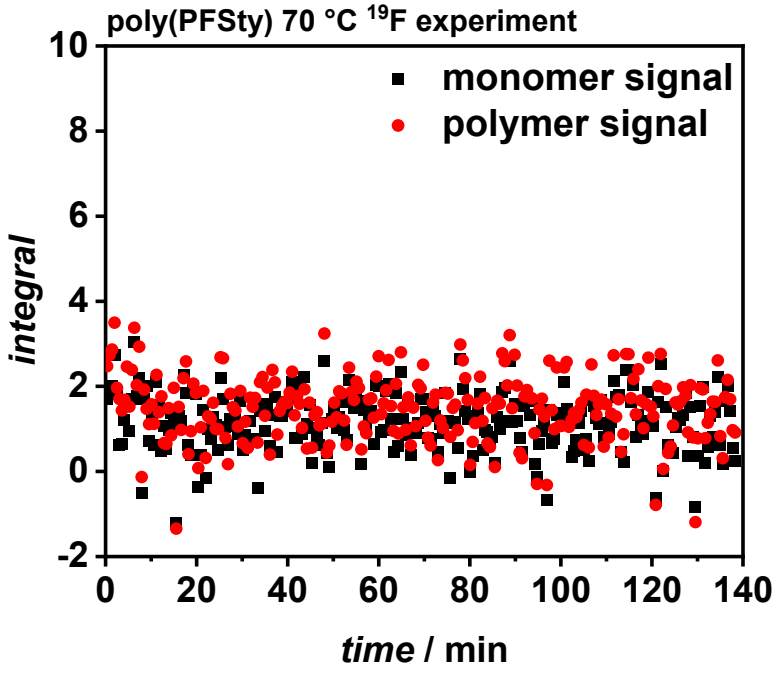

Figure S4. ^{19}F NMR resonance integrals of PFSty and poly(PFSty) over the course of a TT experiment of the RAFT polymerisation at 70 °C recorded on a 60 MHz benchtop NMR device. Monomer and polymer signals could not be resolved for conversion calculations due to an insufficient signal-to-noise ratio.

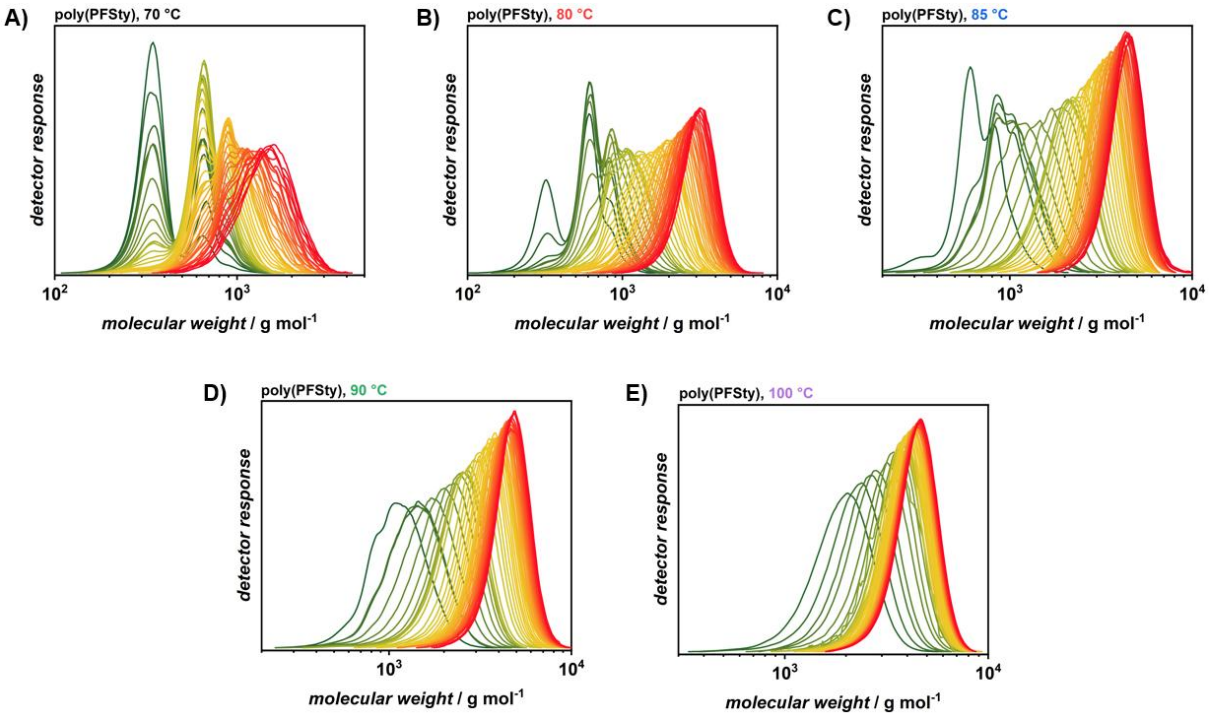

Figure S5. SEC traces of poly(PFSty) recorded by online SEC during the TT experiments at varying temperatures with CPDT as RAFT agent. Calibration: PS.

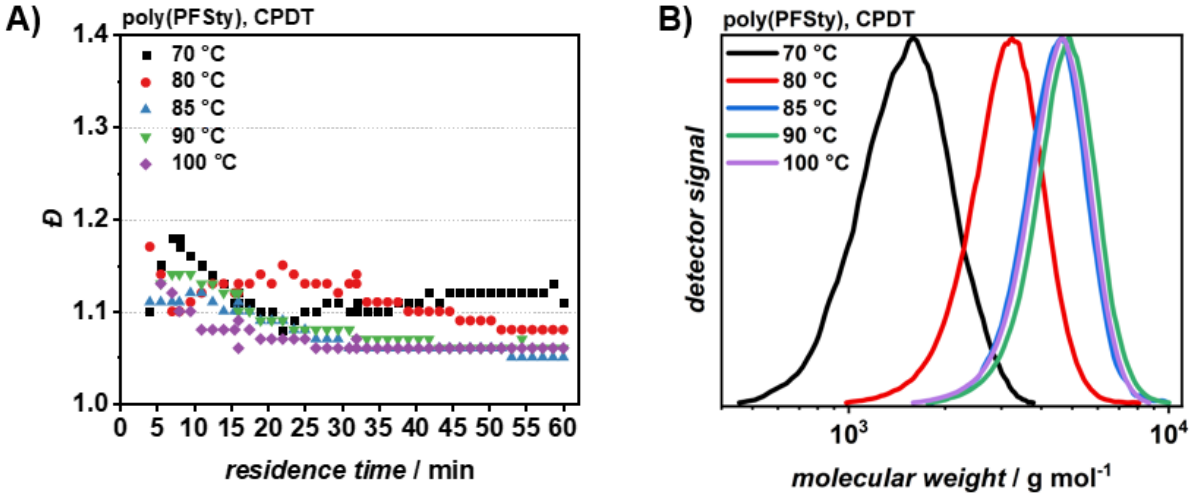

Figure S6. A) Evolution of *Đ* of poly(PFSty)with increasing residence time at different reaction temperatures using CPDT as RAFT agent. B) SEC traces of poly(PFSty) after 60 min of residence time at different temperatures. Calibration: PS.

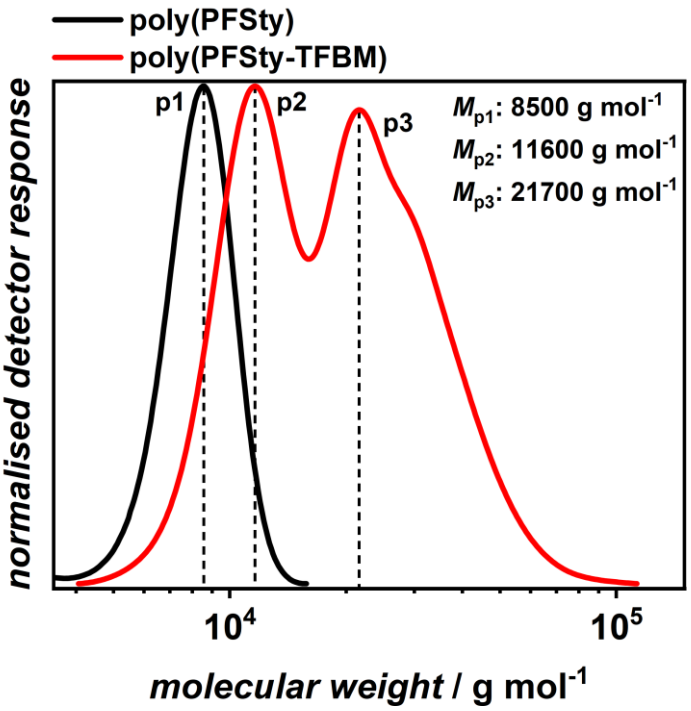

Figure S7. SEC traces of untreated poly(PFSty) before (black) and after (red) PFTR with TFBM. The appearance of p3 at approximately double the molecular weight of p2 indicates dimer formation during the reaction.

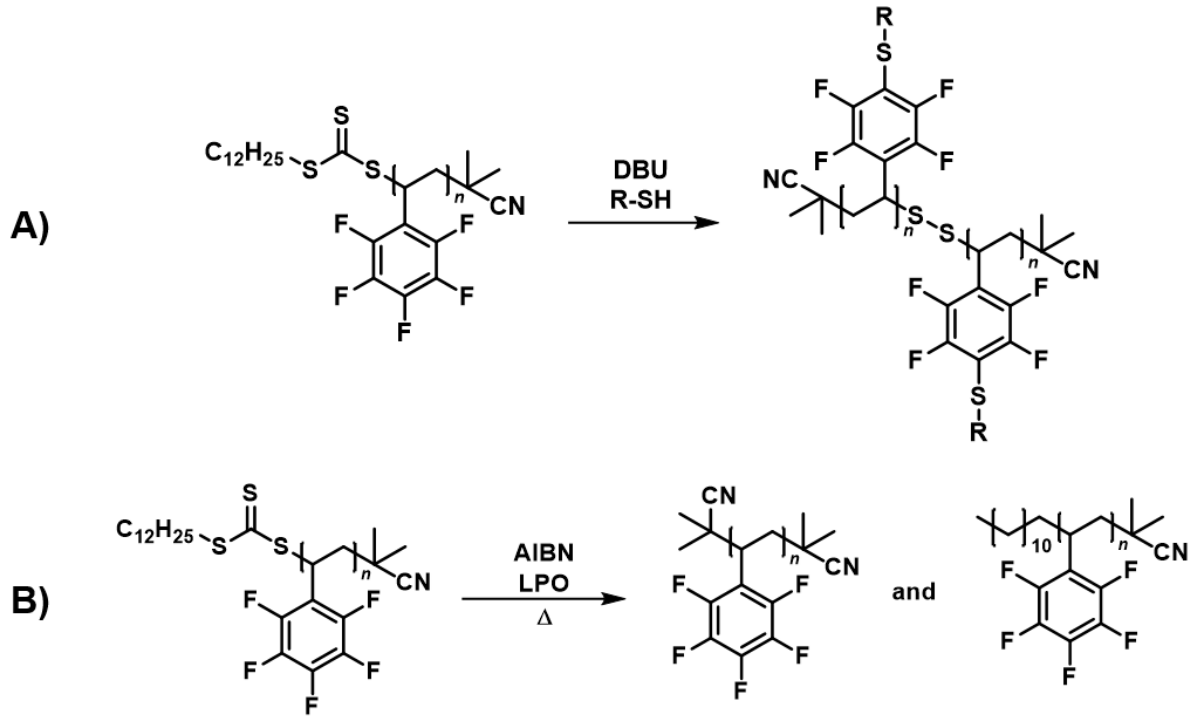

Scheme S1. A) Reaction scheme of the proposed dimerisation of poly(PFSty) during PFTR through disulfide formation facilitated by the RAFT end group. B) Reaction scheme for the cleavage of the RAFT end group by radical transfer using AIBN and LPO as radical source to avoid future polymer dimerisation during PFTR.

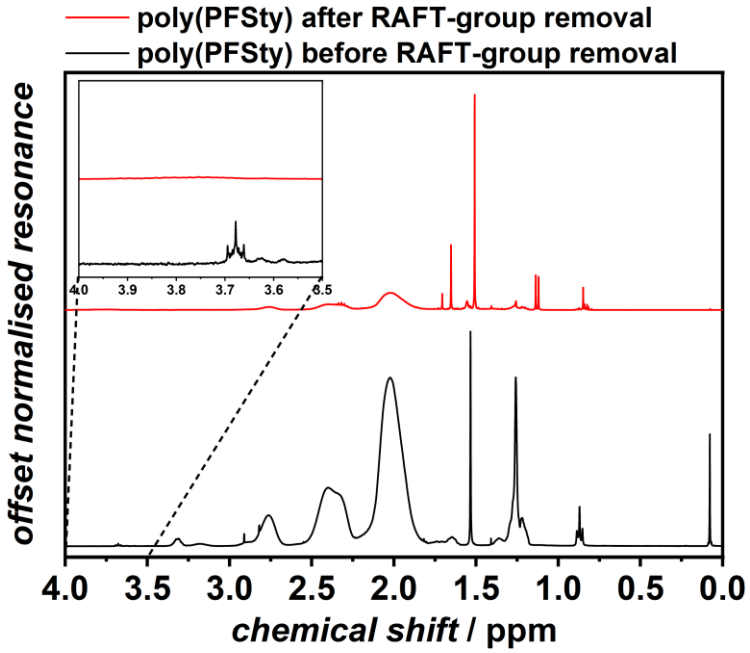

Figure S8. ^{1}H NMR spectra of untreated poly(PFSty) (black) and poly(PFSty) after end group removal with AIBN and LPO (black) in CD_2Cl_2. The inset magnification confirms the removal of RAFT end group through disappearance of S-CH_2 resonances of CPDT.

Details on the flow reactor platform used for flow PFTR experiments

The flow setup was comprised of four CETONI Nemesys M syringe pumps (volumes = 2 x 50 mL and 2 x 25 mL) equipped with a 3-way high-pressure Contiflow ball valve from CETONI GmbH (Korbussen, Germany). All connections were made by stainless steel tubing with an inner diameter of 1/32" (0.8 mm) and streams were combined with Swagelok T- or cross-pieces, respectively. The 3D-printed metal flow reactor made from 316L stainless steel (Type 1.4404) and fabricated by selective laser sintering (SLS). The reactor volume was 1 mL with a flow channel radius of 1.00 mm. The reactor was heated by custom-made heating jackets made from aluminum equipped with 4 heating cartridges (160 W heating power each) with integrated Type K thermocouples from Horst GmbH (Lorsch, Germany). Temperature control was done by a F4T 4-zone benchtop temperature controller from Zesta Engineering Ltd. (Mississauga, ON, USA). The flow reactor was placed inside the heating jackets and screwed together firmly for good contact and heat transfer. For a flow-PFTR with only one thiol, three pumps were used (1 x 50 mL for polymer solution and 2 x 25 mL for thiol and DBU solutions) and the thiol and DBU streams were combined before merging with the polymer stream and leading into the reactor. Mixed flow-PFTR experiments used four syringe pumps (2 x 50 mL for polymer and DBU solutions and 2 x 25 mL for the respective thiols). The thiol streams were merged, and the resulting stream was merged with the DBU stream. This stream was then combined with the polymer stream before feeding into the heated flow reactor.

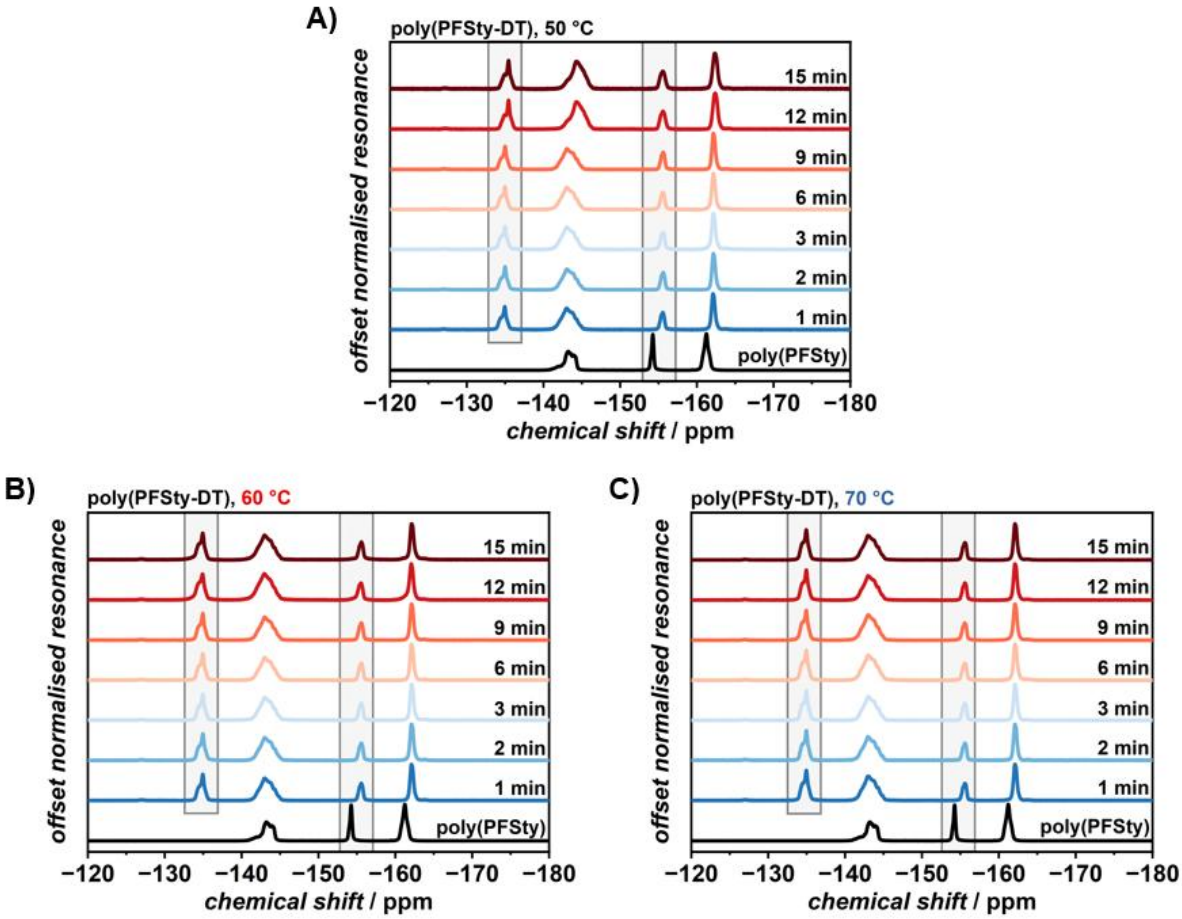

Figure S9. ^{19}F NMR spectra of poly(PFSty) (black) and poly(PFSty-DT) (coloured) made by flow-PFTR at 50 °C (A), 60 °C (B), and 70 °C (C) with increasing residence time. The marked areas represent the regions of chemical shift attributed to *meta* fluorine atoms of poly(PFSty-DT) at around -135 ppm and *para* fluorine atoms of poly(PFSty) at -155 ppm used for conversion calculation.

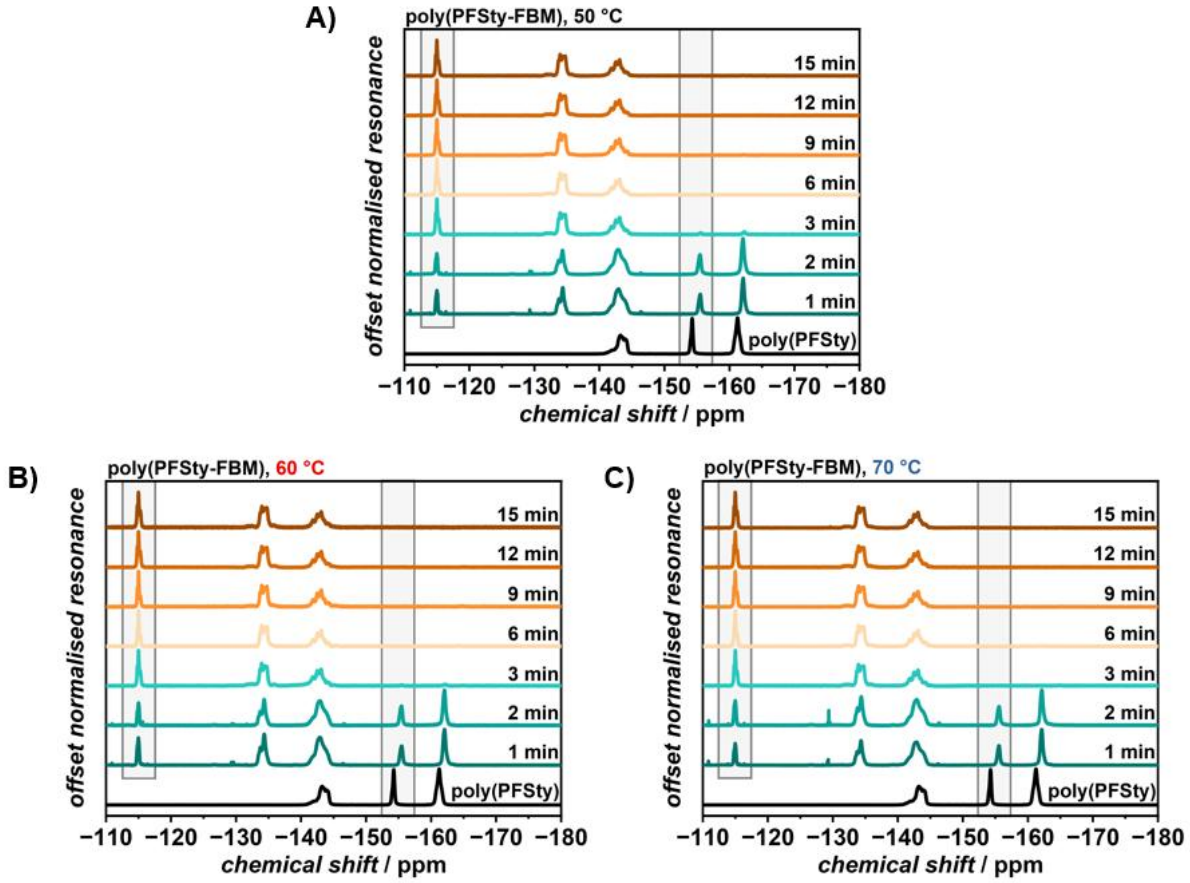

Figure S10. ^{19}F NMR spectra of poly(PFSty) (black) and poly(PFSty-FBM) (coloured) made by flow-PFTR at 50 °C (A), 60 °C (B), and 70 °C (C) with increasing residence time. The marked areas represent the regions of chemical shift attributed to *para* fluorine atoms of FBM in poly(PFSty-FBM) at around -115 ppm and *para* fluorine atoms of poly(PFSty) at -155 ppm used for conversion calculation.

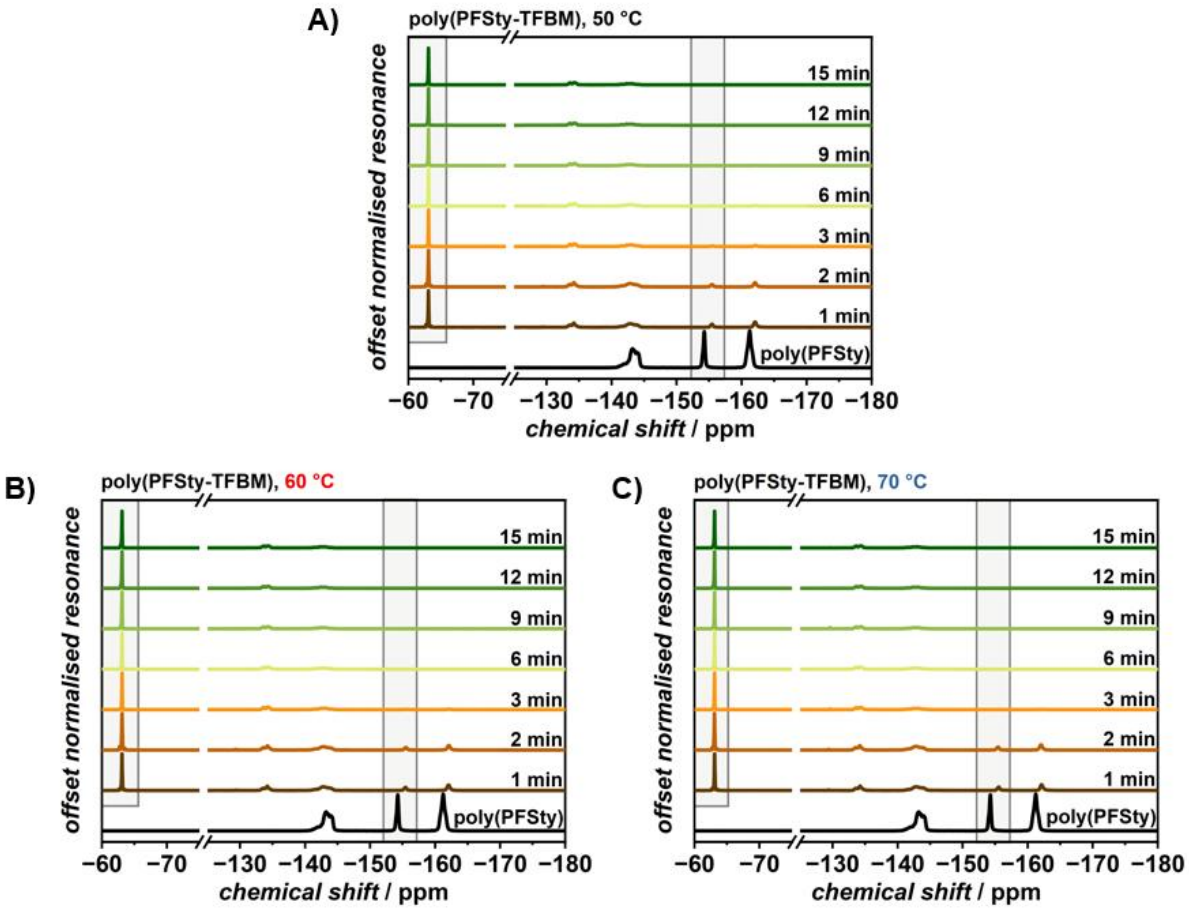

Figure S11. ^{19}F NMR spectra of poly(PFSty) (black) and poly(PFSty-TFBM) (coloured) made by flow-PFTR at 50 °C (A), 60 °C (B), and 70 °C (C) with increasing residence time. The marked areas represent the regions of chemical shift attributed to CF_3 fluorine atoms of TFBM in poly(PFSty-TFBM) at around -63 ppm and *para* fluorine atoms of poly(PFSty) at -155 ppm used for conversion calculation.

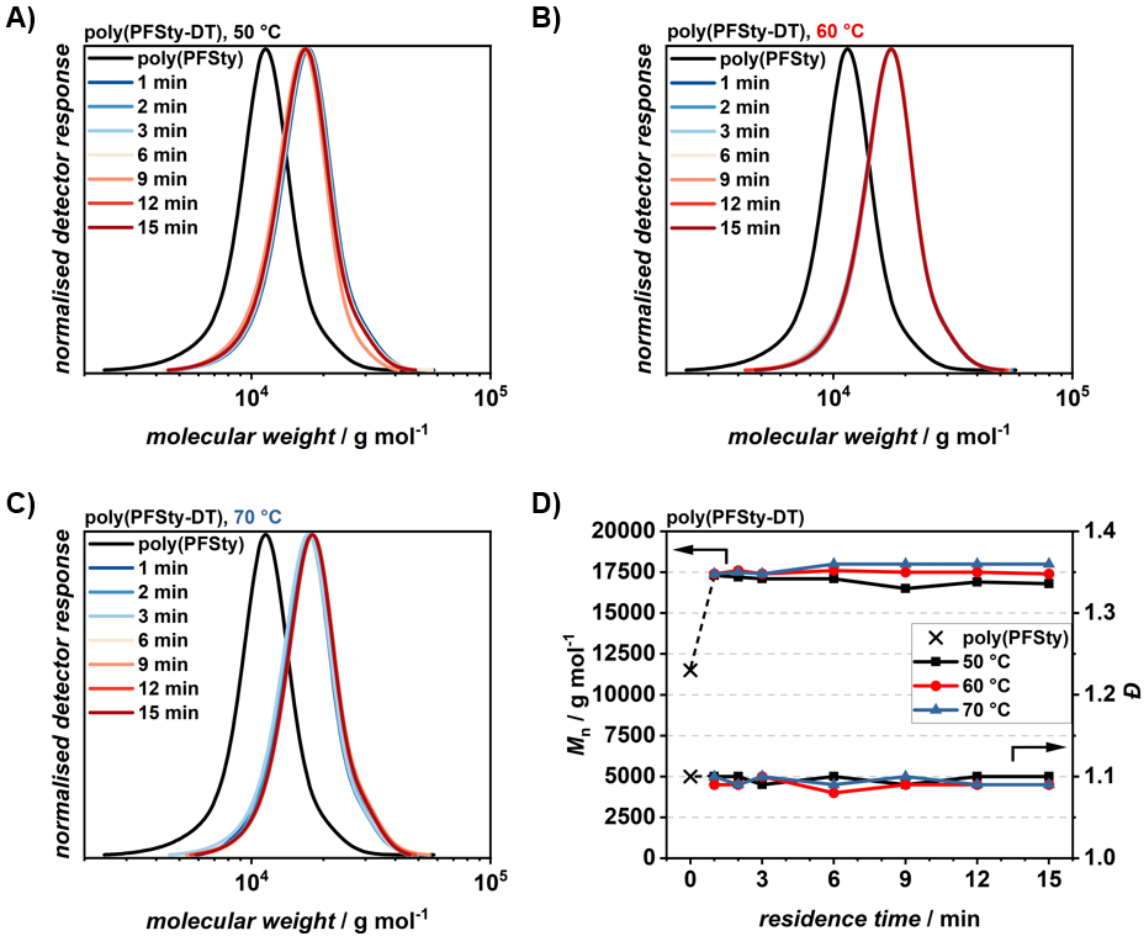

Figure S12. A) – C) SEC traces of poly(PFSty) (black) and poly(PFSty-DT) (coloured) after flow-PFTR with increasing residence time at 50, 60, and 70 °C, respectively. D) M_n and $Đ$ of poly(PFSty-DT) after flow-PFTR with increasing residence time at 50, 60, and 70 °C, respectively. The black X represents M_n and $Đ$ of poly(PFSty) before the reaction. Calibration: PS.

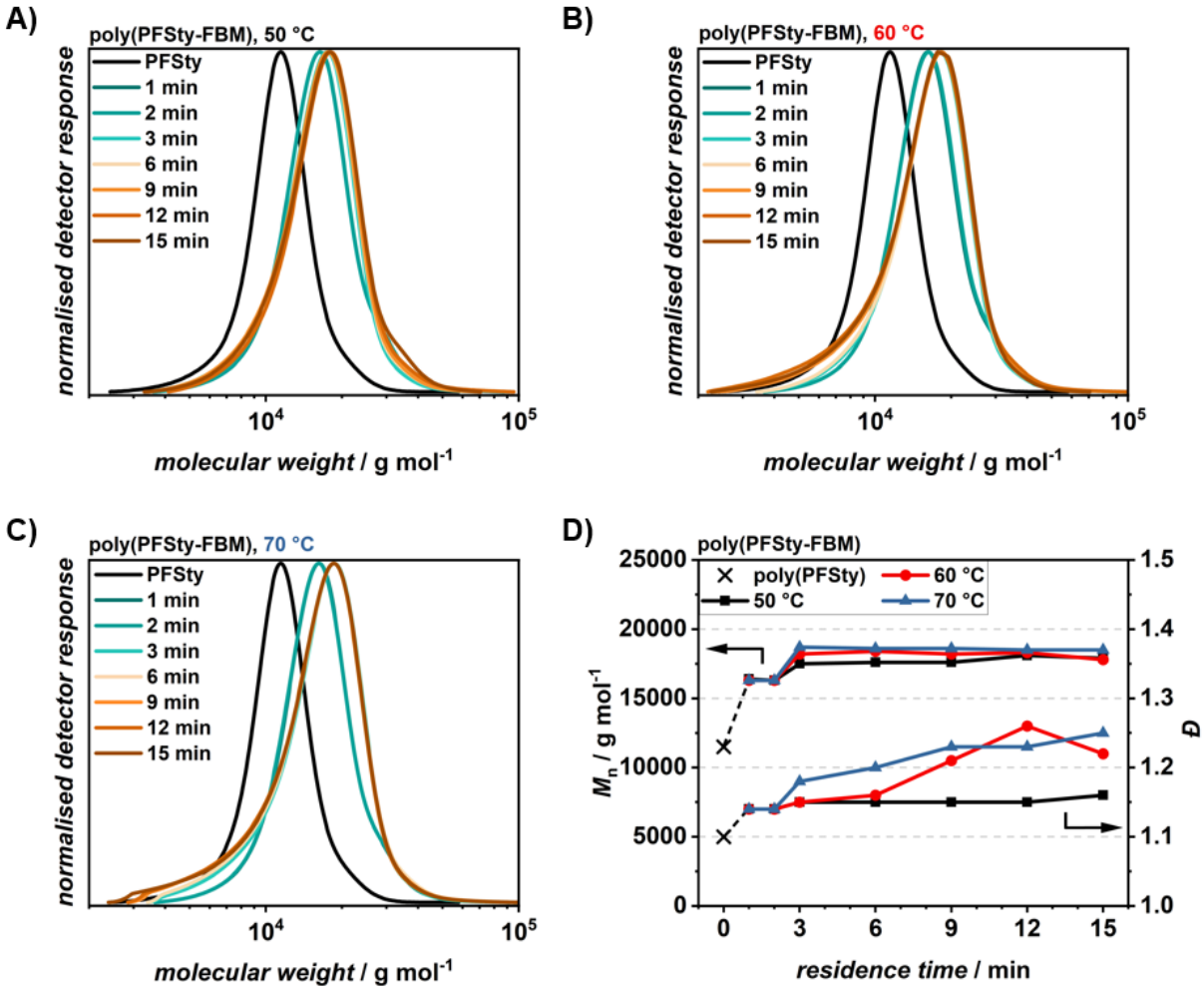

Figure S13. A) – C) SEC traces of poly(PFSty) (black) and poly(PFSty-FBM) (coloured) after flow-PFTR with increasing residence time at 50, 60, and 70 °C, respectively. D) M_n and $Đ$ of poly(PFSty-FBM) after flow-PFTR with increasing residence time at 50, 60, and 70 °C, respectively. The black X represents M_n and $Đ$ of poly(PFSty) before the reaction. Calibration: PS.

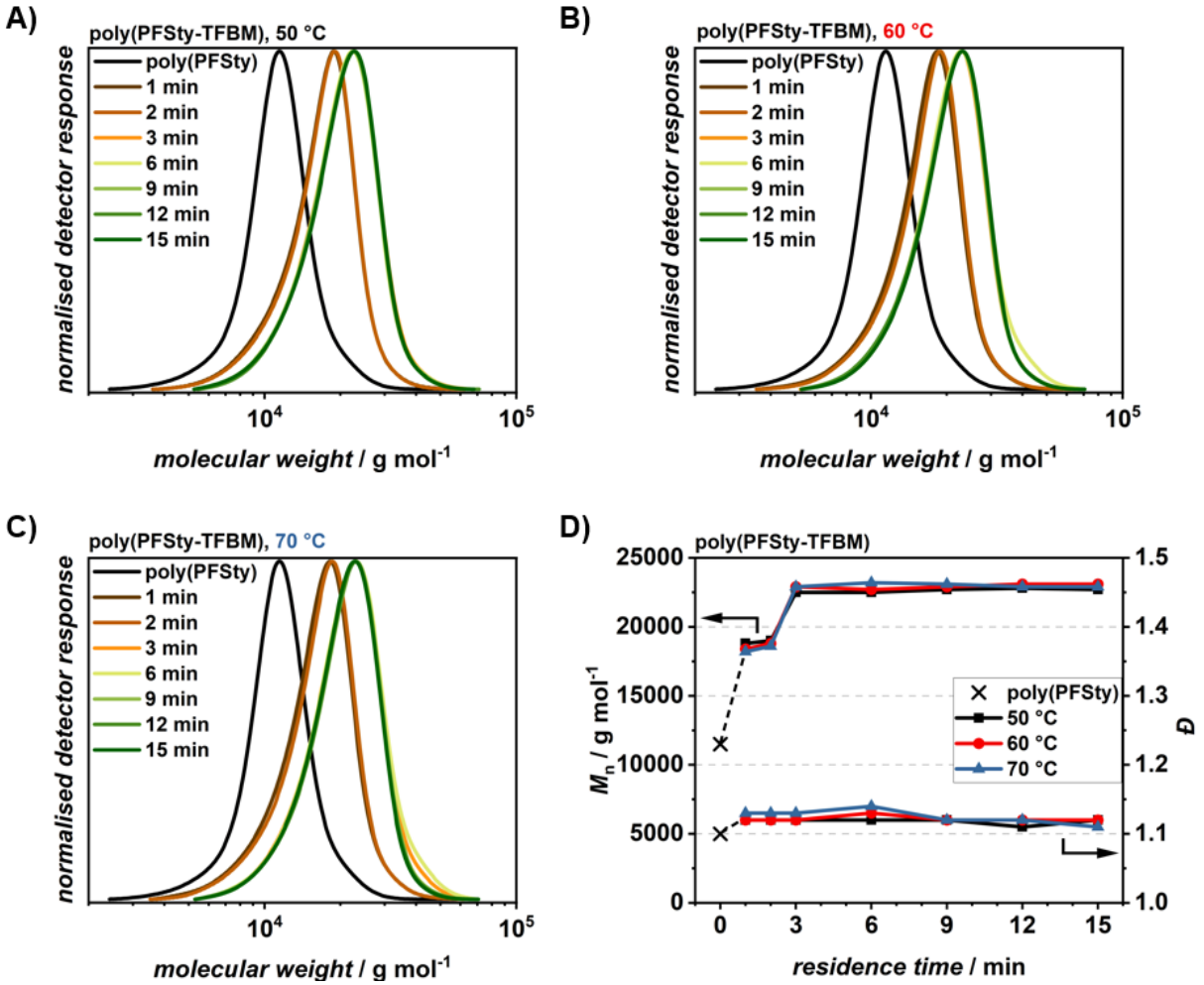

Figure S14. A) – C) SEC traces of poly(PFSty) (black) and poly(PFSty-TFBM) (coloured) after flow-PFTR with increasing residence time at 50, 60, and 70 °C, respectively. D) M_n and $Đ$ of poly(PFSty-TFBM) after flow-PFTR with increasing residence time at 50, 60, and 70 °C, respectively. The black X represents M_n and $Đ$ of poly(PFSty) before the reaction. Calibration: PS.

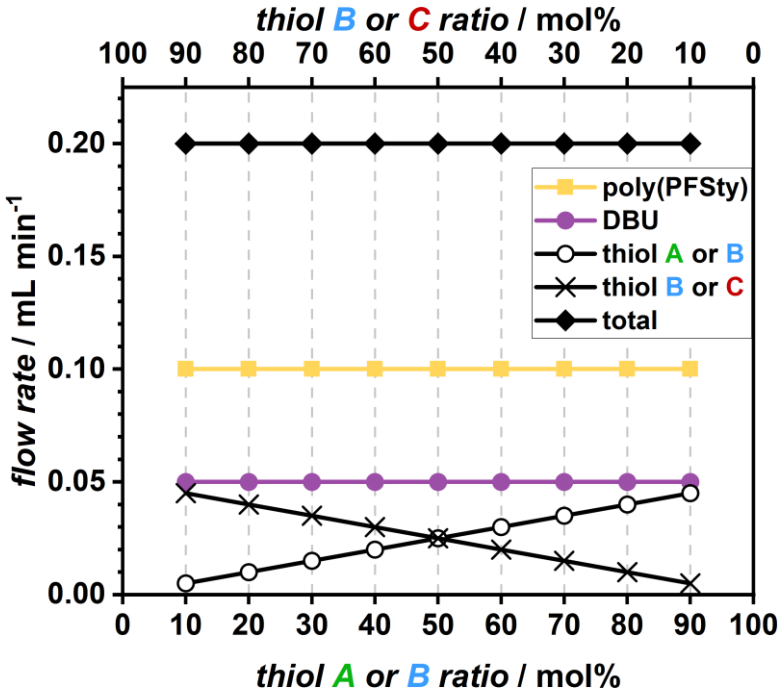

Figure S15. Graphical visualisation of the flow rate relations during a mixed flow-PFTR with two thiols. The total flow rate of 0.20 mL min^{-1} results in a constant residence time of 5 min for all samples at a 1 mL reactor volume. Possible thiol pairs were A – B, A – C, and B – C. When the flow rate of one thiol solution increased, the flow rate of the other thiol solution decreased accordingly to meet the desired molar ratios between both.

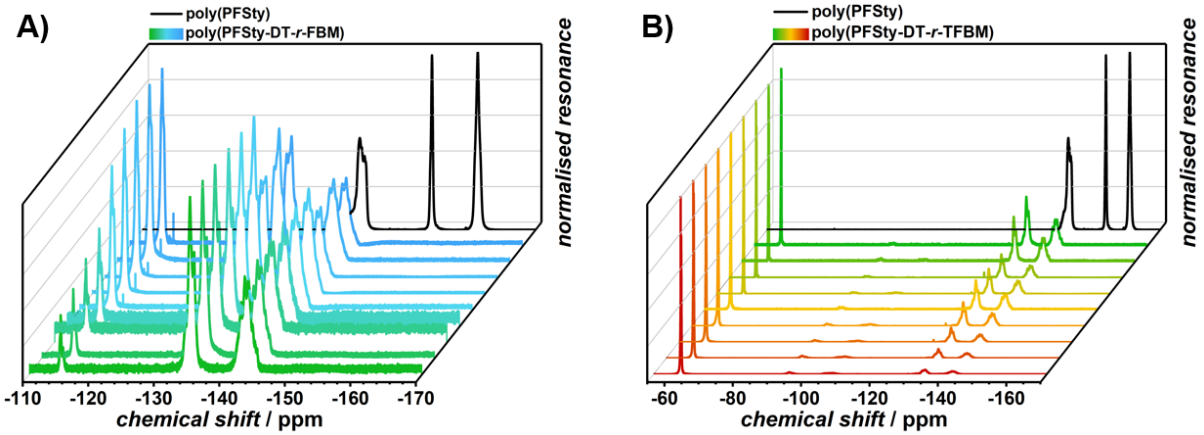

Figure S16. Normalised ^{19}F NMR spectra of poly(PFSty-DT-*r*-FBM) (A) and poly(PFSty-DT-*r*-TFBM) (B) with poly(PFSty) (black). Disappearance of *para* fluorine atoms of poly(PFSty) and shift of *ortho* and *meta* fluorine atoms confirm the full conversion of active groups during the mixed flow-PFTR experiments.

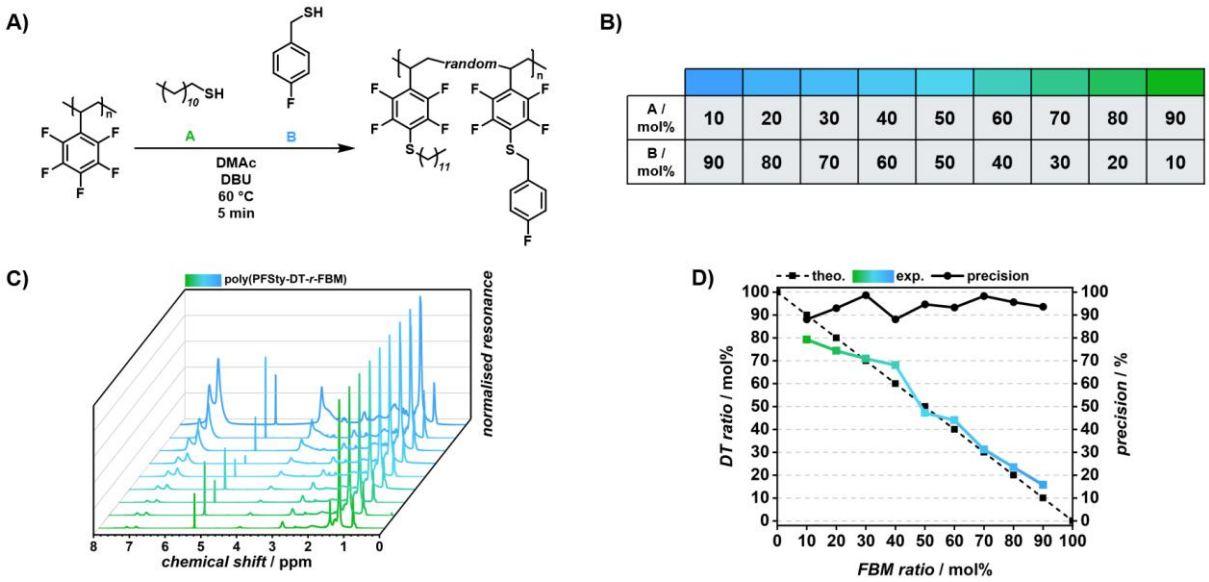

Figure S17. A) Reaction scheme of the mixed flow-PFTR of poly(PFSty) with DT and FBM. B) Colour-code for the PPM of poly(PFSty) with 10 – 90 mol% DT and 90 – 10 mol% FBM, respectively. C) Normalised ^{1}H NMR spectra of poly(PFSty-DT-*r*-FBM). The left peaks at 6.5 – 7.5 ppm are attributed to the aromatic protons of FBM while the peak at 0.88 ppm is attributed to the CH_3 group of DT, respectively. D) Theoretical and experimental modification ratios of poly(PFSty) with DT and FBM, respectively. The black dashed line represents the theoretical input ratios of DT and FBM which are directly linked to the flow rates of the reactor setup while the coloured solid line represents the found ratios in the final polymers. The precision (black circles) was between 88 and 99 % depending on the thiol ratio.

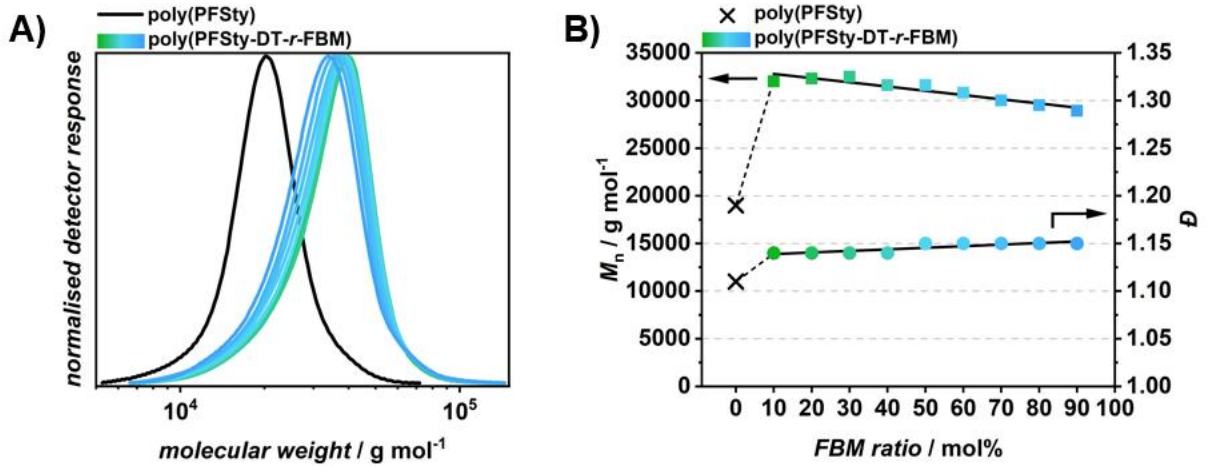

Figure S18. SEC traces (A) and M_n and $Đ$ (B) of poly(PFSty) (black) and poly(PFSty-DT-*r*-FBM) (coloured) with changing thiol ratios. As the FBM ratio increased, the DT ratio decreased accordingly. Calibration: PS.

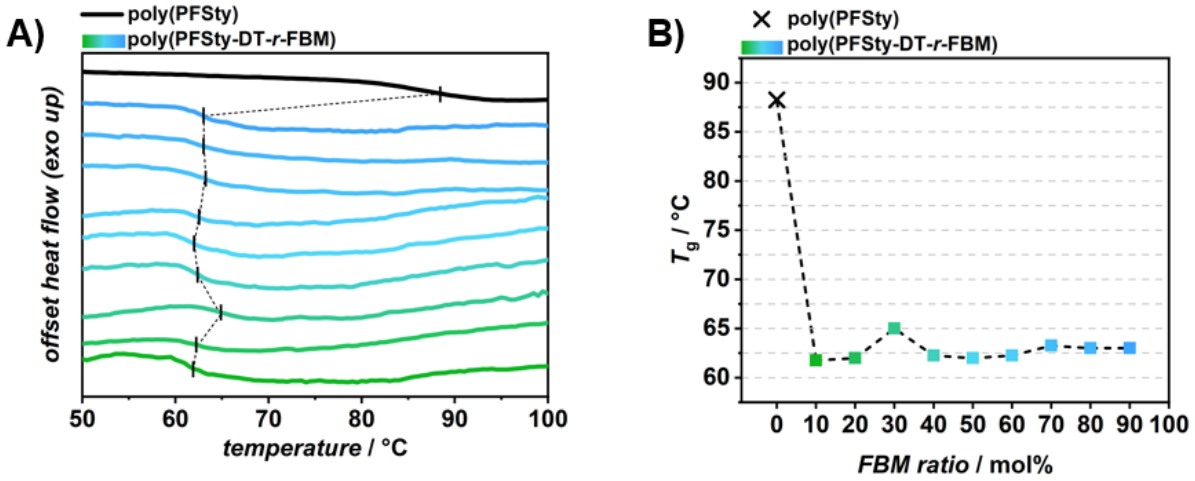

Figure S19. DSC thermograms (A) and T_gs (B) of poly(PFSty) (black) and poly(PFSty-DT-*r*-FBM) (coloured) with changing thiol ratios. As the FBM ratio increased, the DT ratio decreased accordingly. Heating rate: 10 K min^{-1}.

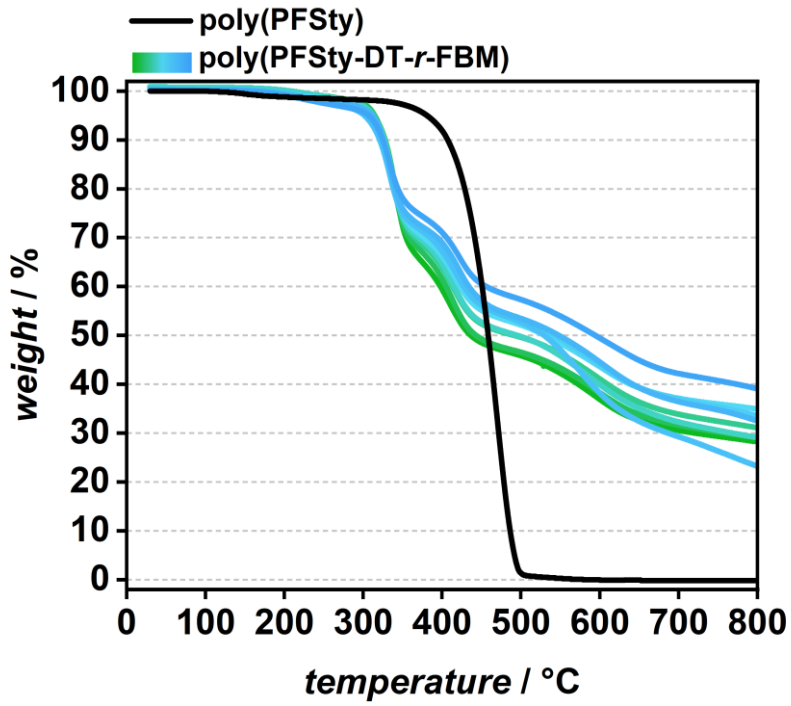

Figure S20. Thermal decomposition profiles of poly(PFSty) (black) and poly(PFSty-DT-*r*-FBM) up to 800 °C. Heating rate: 10 K min^{-1}.

Table S5. $T_{5\%}$ and residual weight at 800 °C of poly(PFSty) and poly(PFSty-DT-*r*-FBM) determined by TGA.

polymer	$T_{5\%}$ / °C	*weight at 800 °C* / wt%
poly(PFSty)	381	0
poly(PFSTy-DT$_{10}$-*r*-FBM$_{90}$)	307	39
poly(PFSTy-DT$_{20}$-*r*-FBM$_{80}$)	312	33
poly(PFSTy-DT$_{30}$-*r*-FBM$_{70}$)	302	23
poly(PFSTy-DT$_{40}$-*r*-FBM$_{60}$)	311	34
poly(PFSTy-DT$_{50}$-*r*-FBM$_{50}$)	309	35
poly(PFSTy-DT$_{60}$-*r*-FBM$_{40}$)	313	29
poly(PFSTy-DT$_{70}$-*r*-FBM$_{30}$)	312	31
poly(PFSTy-DT$_{80}$-*r*-FBM$_{20}$)	315	29
poly(PFSTy-DT$_{90}$-*r*-FBM$_{10}$)	313	28

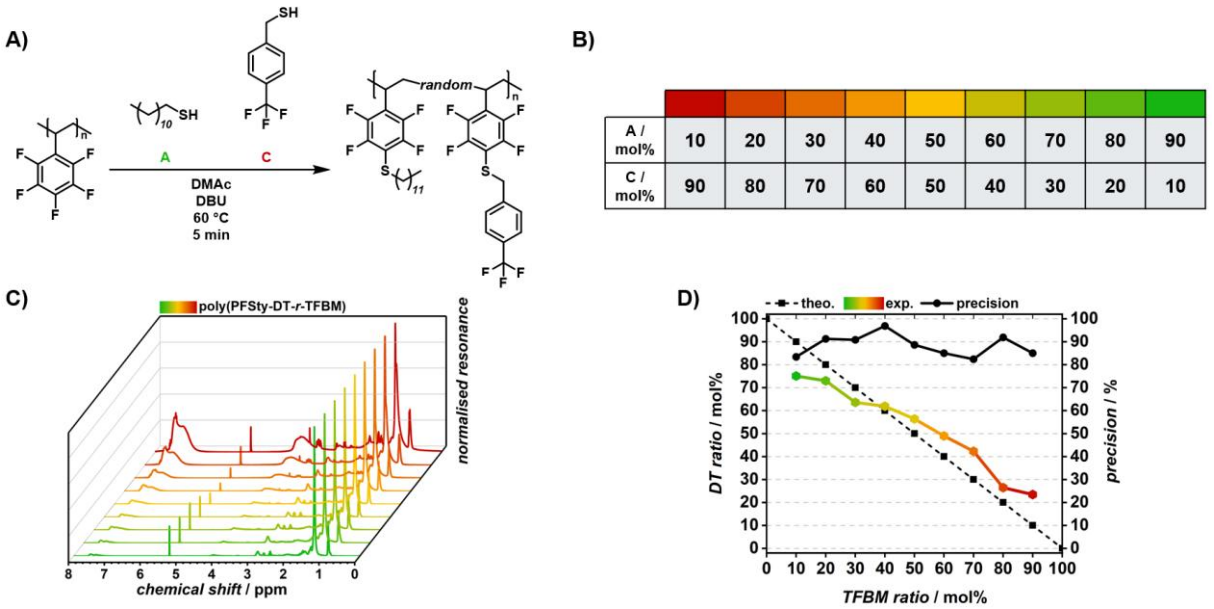

Figure S21. A) Reaction scheme of the mixed flow-PFTR of poly(PFSty) with DT and TFBM. B) Colour-code for the PPM of poly(PFSty) with 10 – 90 mol% DT and 90 – 10 mol% TFBM, respectively. C) Normalised ^{1}H NMR spectra of poly(PFSty-DT-*r*-TFBM). The left peaks at 6.5 – 7.5 ppm are attributed to the aromatic protons of TFBM while the peak at 0.88 ppm is attributed to the CH_3 group of DT, respectively. D) Theoretical and experimental modification ratios of poly(PFSty) with DT and TFBM, respectively. The black dashed line represents the theoretical input ratios of DT and TFBM which are directly linked to the flow rates of the reactor setup while the coloured solid line represents the found ratios in the final polymers. The precision (black circles) was between 82 and 97 % depending on the thiol ratio.

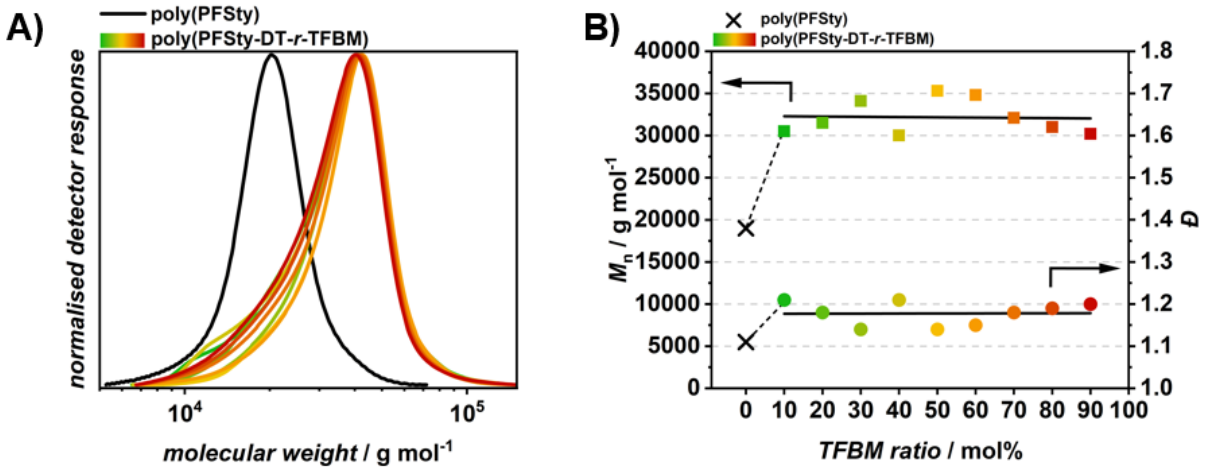

Figure S22. SEC traces (A) and M_n and $Đ$ (B) of poly(PFSty) (black) and poly(PFSty-DT-*r*-TFBM) (coloured) with changing thiol ratios. As the TFBM ratio increased, the DT ratio decreased accordingly. Calibration: PS.

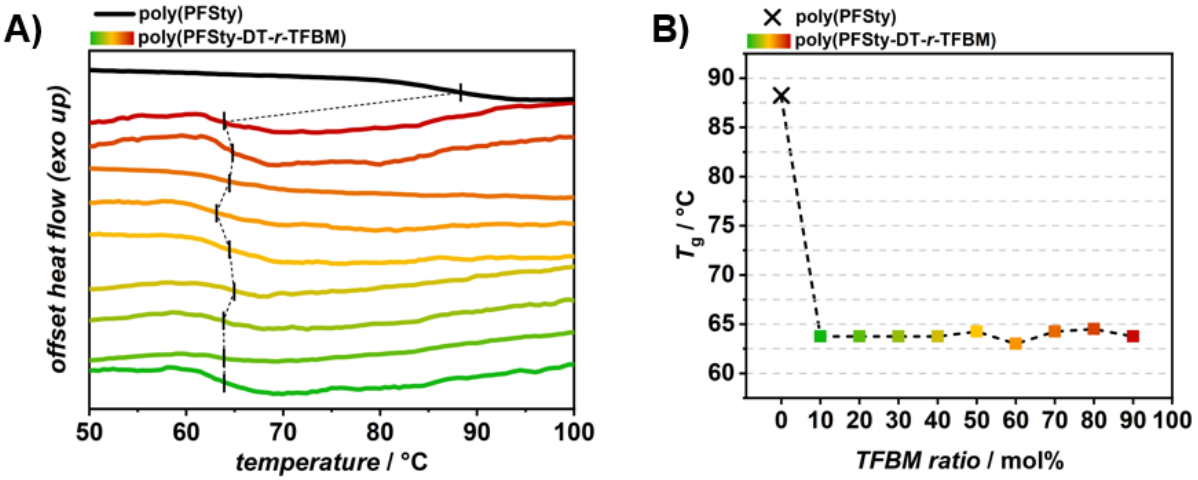

Figure S23. DSC thermograms (A) and T_gs (B) of poly(PFSty) (black) and poly(PFSty-DT-*r*-TFBM) (coloured) with changing thiol ratios. As the TFBM ratio increased, the DT ratio decreased accordingly. Heating rate: 10 K min^{-1}.

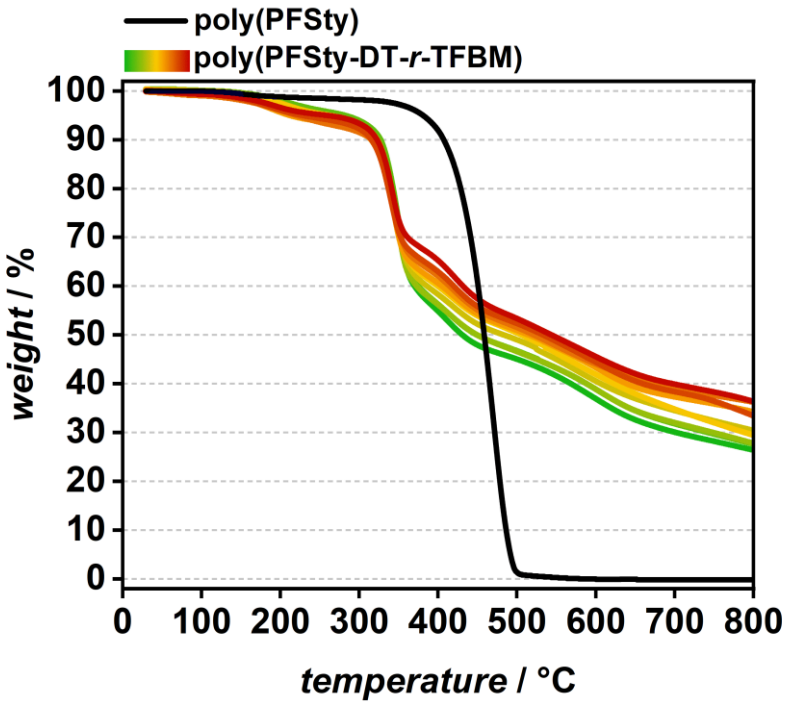

Figure S24. Thermal decomposition profiles of poly(PFSty) (black) and poly(PFSty-DT-*r*-TFBM) up to 800 °C. Heating rate: 10 K min^{-1}.

Table S6. $T_{5\%}$ and residual weight at 800 °C of poly(PFSty) and poly(PFSty-DT-*r*-TFBM) determined by TGA.

polymer	$T_{5\%}$ / °C	*weight at 800 °C* / wt%
poly(PFSty)	381	0
poly(PFSTy-DT_{10}-*r*-$TFBM_{90}$)	259	36
poly(PFSTy-DT_{20}-*r*-$TFBM_{80}$)	227	34
poly(PFSTy-DT_{30}-*r*-$TFBM_{70}$)	220	36
poly(PFSTy-DT_{40}-*r*-$TFBM_{60}$)	211	34
poly(PFSTy-DT_{50}-*r*-$TFBM_{50}$)	263	30
poly(PFSTy-DT_{60}-*r*-$TFBM_{40}$)	253	31
poly(PFSTy-DT_{70}-*r*-$TFBM_{30}$)	262	28
poly(PFSTy-DT_{80}-*r*-$TFBM_{20}$)	282	28
poly(PFSTy-DT_{90}-*r*-$TFBM_{10}$)	244	27

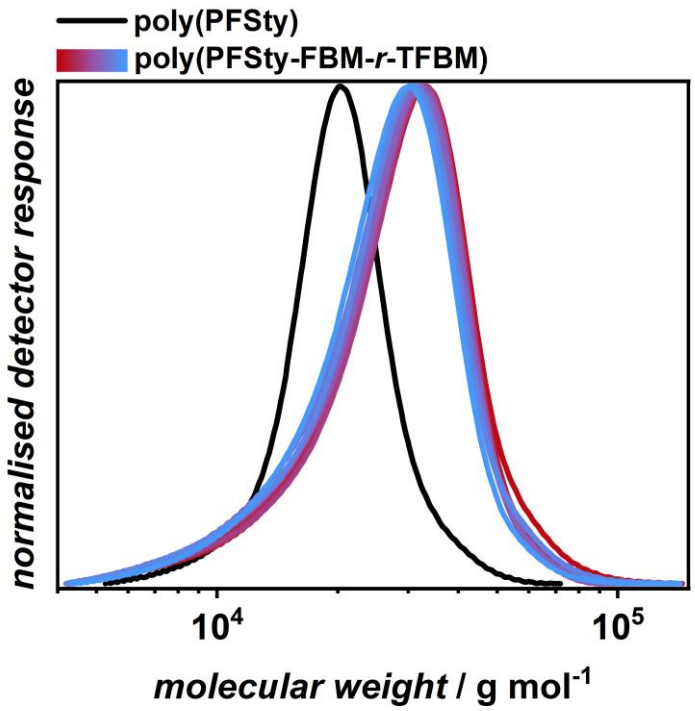

Figure S25. SEC traces of poly(PFSty) (black) and poly(PFSty-DT-*r*-TFBM) (coloured). Calibration: PS.

Table S7. $T_{5\%}$ and residual weight at 800 °C of poly(PFSty) and poly(PFSty-FBM-*r*-TFBM) determined by TGA.

polymer	$T_{5\%}$ / °C	*weight at 800 °C* / wt%
poly(PFSty)	381	0
poly(PFSTy-FBM$_{10}$-*r*-TFBM$_{90}$)	323	31
poly(PFSTy-FBM$_{20}$-*r*-TFBM$_{80}$)	323	32
poly(PFSTy-FBM$_{30}$-*r*-TFBM$_{70}$)	323	33
poly(PFSTy-FBM$_{40}$-*r*-TFBM$_{60}$)	323	34
poly(PFSTy-FBM$_{50}$-*r*-TFBM$_{50}$)	320	35
poly(PFSTy-FBM$_{60}$-*r*-TFBM$_{40}$)	321	33
poly(PFSTy-FBM$_{70}$-*r*-TFBM$_{30}$)	320	32
poly(PFSTy-FBM$_{80}$-*r*-TFBM$_{20}$)	320	34
poly(PFSTy-FBM$_{90}$-*r*-TFBM$_{10}$)	319	31

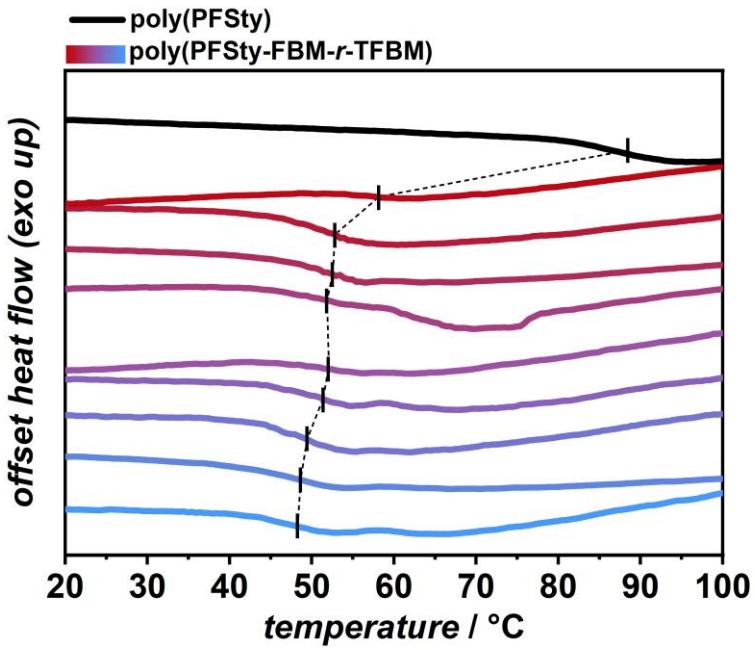

Figure S26. DSC thermograms of poly(PFSty) (black) and poly(PFSty-FBM-*r*-TFBM) (coloured) with changing thiol ratios. Heating rate: 10 K min^{-1}.

References

[1] J. van Herck and T. Junkers, *Chem. Methods*, 2022, **2**, e202100090.